Journal of Luminescence 173 (2016) 263–273

Contents lists available at ScienceDirect

Journal of Luminescence

journal homepage: www.elsevier.com/locate/jlumin

Full Length Article

Investigation of the quenching mechanisms of Tb^{3+} doped scheelites

Katrien W. Meert [a,b], Jonas J. Joos [a,b], Dirk Poelman [a,b], Philippe F. Smet [a,b,*]

[a] Lumilab, Department of Solid State Sciences, Ghent University, Krijgslaan 281 - S1, Ghent, Belgium
[b] Center for Nano and Biophotonics (NB Photonics), Ghent University, Ghent, Belgium

ARTICLE INFO

Article history:
Received 14 August 2015
Received in revised form
22 December 2015
Accepted 25 December 2015
Available online 1 January 2016

Keywords:
Luminescence
Scheelite
Terbium
Thermal quenching

ABSTRACT

The luminescence of terbium-doped lead tungstate ($PbWO_4:Tb^{3+}$) features not only emission from the $^5D_4$ and $^5D_3$ excited states of Tb^{3+}, but also host and defect related broad emission bands are found. The blue host emission is attributed to the WO_4^{2-} centres whereas the green emission can be ascribed to WO_3 defects. Upon host excitation, Tb^{3+} emission is observed pointing to energy transfer mechanisms between host and dopants. The electronic structure of Tb^{3+} defects inside the $PbWO_4$ host are empirically deduced from optical and luminescence spectroscopy, both in steady-state as well as in time-resolved mode, as a function of temperature and doping concentration to asses the influence of key parameters in the energy transfer processes. The luminescence originating from Tb^{3+} ions shows a strong dependency on both the excitation wavelength and the temperature. For instance, an intensity increase in the 75–125 K range upon excitation via the WO_4^{2-} centres is found, which is absent for direct

Investigation of the quenching mechanisms of Tb^{3+} doped scheelites

Katrien W. Meert[a, b], Jonas J. Joos[a, b], Dirk Poelman[a, b], Philippe F. Smet[a, b, *]
[a]Lumilab, Department of Solid State Sciences, Ghent University, Krijgslaan 281 - S1, Ghent, Belgium
[b]Center for Nano and Biophotonics (NB Photonics), Ghent University, Ghent, Belgium
*corresponding author: philippe.smet@ugent.be

Abstract: The luminescence of terbium doped lead tungstate ($PbWO_4$:Tb^{3+}) features not only emission from the $^5D_4$ and $^5D_3$ excited states of Tb^{3+}, but also host and defect related broad emission bands are found. The blue host emission is attributed to the WO_4^{2-} centres whereas the green emission can be ascribed to WO_3 defects. Upon host excitation, Tb^{3+} emission is observed pointing to energy transfer mechanisms between host and dopants. The electronic structure of Tb^{3+} defects inside the $PbWO_4$ host are empirically deduced from optical and luminescence spectroscopy, both in steady-state as well as in time-resolved mode, as a function of temperature and doping concentration to asses the influence of key parameters in the energy transfer processes. The the luminescence originating from Tb^{3+} ions shows a strong dependency on both the excitation wavelength and the temperature. For instance, an intensity increase in the 75 K to 125 K range upon excitation via the WO_4^{2-} centres is found, which is absent for direct excitation. The undoped sample is characterized by a temperature dependent energy transfer from WO_4^{2-} to WO_3 defect centres with an thermal energy barrier of 0.26 eV. The divergent thermal quenching profiles of the host emission for pure $PbWO_4$ versus doped materials reveal both a direct energy transfer and a temperature dependent energy transfer process from the host towards the Tb^{3+} ions. The emission efficiency of the ^5D_J levels is investigated as well and a thermal quenching energy of 0.51 eV (J = 3) and 0.86 eV (J = 4) was found.
keywords: Luminescence, Scheelite, Terbium, Thermal quenching, Energy transfer

1 Introduction

Trivalent lanthanide ions are known for their atomic-like line spectra and long lifetime, both arising from the 4f-4f character of the luminescent transitions. As the relative energies of the multiplets hardly shift upon doping in the host material due to the shielding electrons of the filled $5s^2$ and $5p^6$ shells, each ion is linked with specific energy transitions, e.g. Eu^{3+} shows red emission whereas Tb^{3+} spectra are blue and or green [1, 2]. Apart from its emission energy, the relative position and number of energy levels are crucial for the feasibility of the material. Too many close lying energy levels, like in the case of Sm^{3+}, results in dominating relaxation and transfer processes with an increasing possibility of quenching and low emission efficiency as a consequence. On the other hand, specific energy gaps can be beneficial for some applications. For example, couples of Tb^{3+} - Yb^{3+} ions show near-infrared quantum cutting and are therefore useful in downconversion layers for silicon solar cells [3]. In general, lanthanide ions in solids have shown their applicability in many fields including light emitting diodes, fluorescent lamps, displays and temperature sensors [4, 5, 6, 7].

In the Tb^{3+} ion, characteristic radiative electronic transitions occur from the $^5D_4$ and $^5D_3$ multiplets towards the lower-lying ^7F_J multiplets within the $4f^8$ configuration. As dopant, the Tb^{3+} ion can be photo-excited in different ways:

- By an internal transition within the $4f^8$ configuration.
- By an internal interconfigurational $4f^8$-$4f^75d^1$ transition [8].
- By a charge transfer transition. An electron is then removed or added to the 4f shell of the Tb^{3+} ion. For the case where an electron is added, typically coming from a nearest neighbor anion, often no specific name for this charge transfer (CT) is used, however

sometimes referred to as a Ligand - to - Metal Charge Transfer state (LMCT) [9]. On the other hand, when an electron is removed from the 4f shell, being transferred to the unfilled nd shell of a nearby transition metal ion, this phenomenon is often referred to as an intervalence charge transfer, although this name was initially reserved for homonuclear MMCT states by the IUPAC [10, 11, 12].

- The energy of an electron-hole pair can be transferred to a Tb^{3+} defect. Electron-hole pairs can only be created when the photon energy of the excitation light exceeds the host's band gap energy [13].
- If defects, other than Tb^{3+} dopants under study, are present in the material, energy absorbed by the additional defect can be transferred to the Tb^{3+} ion if the distance between both is sufficiently small and a spectral overlap exists between both defects [14].

These different kinds of electronic transitions take place between energy levels. When the relevant energy levels are accurately known, not only the interpretation of electronic transitions can be facilitated, but also their response to external parameters such as temperature can be assessed. In reality, obtaining accurate energy levels schemes is not straightforward due to overlapping spectral features and the presence of radiative and non-radiative energy transfer paths, which are often temperature dependent.

Additionally, when two Tb^{3+} ions are sufficiently close to each other, energy transfer between both ions can occur via a quasi-resonant cross relaxation process as the large energy difference of $\pm 0.72\,\mathrm{eV}$ between the $^5D_4$ and $^5D_3$ multiplets excludes multiphonon relaxation at moderate temperature. If cross relaxation takes place, $^5D_4$ emission can be observed upon direct excitation of the $^5D_3$ multiplet [15, 16].

The host material under study, $PbWO_4$, is a member of the scheelite family [17]. It crystallizes in different polymorphs of which two exist as mineral, i.e. tetragonal stolzite and monoclinic raspite. In this work, the former polymorph is investigated. The stolzite structure (space group $I4_1/a$) is characterized by a unit cell with one lead and one tungsten Wyckoff site, both exhibiting the S_4 point symmetry of the distorted dodecahedron, typical for scheelites [18].

When interstitial incorporation is discarded, the Tb optical dopant can be incorporated in the $PbWO_4$ structure in two possible ways, i.e. substituting for a Pb^{2+} (r = 1.33) cation or substituting for a W^{6+} (r = 0.74) cation. From ionic conductivity measurements, Groeninck and Binsma found that a Y^{3+} dopant occupies a tungsten site rather than a lead site, and increases the concentration of oxygen vacancies as a consequence of charge compensation [19, 20]. As Tb^{3+} (r = 1.06) has a very similar ionic radius as well as chemical behavior than Y^{3+} (r = 1.04), this argument assigns the Tb^{3+} defect to a W site in the $PbWO_4$ crystal. However, Takai *et al.* ascribe the oxide ion conduction to the interstitial oxide ions caused by substitution of the aliovalent element Tb in the Pb site [21]. The general opinion favours the occupation of the Tb^{3+} ion at the Pb site in the $PbWO_4$ crystal [22, 23, 24, 25].

Optical spectroscopy of undoped $PbWO_4$ crystals has been performed by multiple authors because of their potential application as scintillation material [26, 27, 28]. Groenink and Blasse elaborated on the early work of Kröger and Van Loo [19]. They found two emission bands which were assigned as blue (peaking around 3.10 eV) and green (peaking around 2.40 eV). The blue emission was attributed to transitions within WO_4^{2-} centres, i.e. radiative annihilation of self-trapped excitons. These charge transfer transitions are thus responsible for the optical band gap of pure $PbWO_4$ crystals. The green emission band is excited at energies below the optical band gap and related to defect emission from an isolated oxygen vacancy, i.e. a WO_3 centre [19]. Babin *et al.* distinguished two green emission bands, one arising from WO_4^{2-} centres in the close

vicinity of lead - deficient regions and one arising from WO_3 centres [29]. Besides these blue and green luminescent centres, emission is observed attributed to other luminescent centres e.g. a centre originating from the presence of Pb^{3+} in $PbWO_4$. This leads to a shift of the oxygen ions and the creation of an vacancy which lowers the symmetry of this WO_3 centre, leading to a red shift of the energy levels. Another type of defects is related to the presence of molybdenum impurities in the material [30].

Interconfigurational $4f^8$-$4f^75d^1$ transitions of Tb^{3+} are not expected to play a role in the luminescence and excited state dynamics of $PbWO_4$:Tb^{3+}. In the case of Ce^{3+} doping in the same host, the 5d level of the Ce^{3+} ion is estimated $3.4 - 3.5\,eV$ above its 4f ground state. If a constant redshift of the 5d level in the $PbWO_4$ host as a function of trivalent lanthanide dopant is assumed, the energy of the local $4f^8$-$4f^75d^1$ transition in $PbWO_4$:Tb^{3+} is expected at about $5.1\,eV$, which is larger than the optical band gap of the host [8, 26, 31].

Novosad *et al.* investigated luminescence of $PbWO_4$: Tb^{3+} with synchrotron and laser radiation and attributed the origin of the host emission to an exciton in the WO_4^{2-} groups at regular sites (blue host emission) and at defect sites (green defect emission). In addition they observed $^5D_4$ emission from Tb^{3+} [32]. Nikl *et al.* investigated the scintillation properties of $PbWO_4$ with different dopants including Tb^{3+}, Sm^{3+} and Pr^{3+} [31].

Hereafter, the temperature dependence of the luminescence output and the decay profiles of Tb^{3+} doped scheelites are investigated for different excitation wavelengths and Tb concentrations. Measurements are performed on four different samples: $PbWO_4$ without intentionally introduced impurities and $PbWO_4$:Tb^{3+} with doping concentrations of 1%, 2% and 5%. The non-doped sample will allow to investigate the host-related characteristics, as a good knowledge of the excited states of the host crystal is necessary for a further correct assignment of the various luminescent characteristics of the Tb doped compounds.

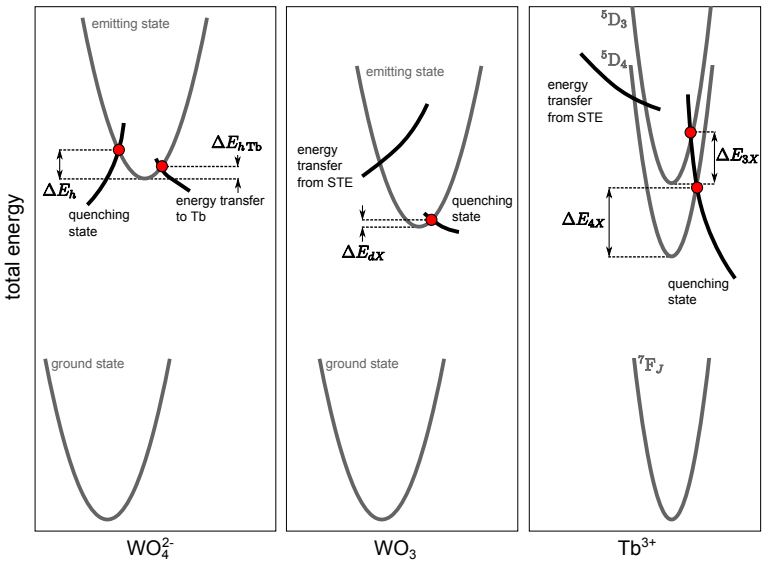

Figure 1: Configurational coordinate diagrams of the WO_4^{2-}, WO_3 and Tb^{3+} centres in $PbWO_4$. This figure serves as a conceptual guide while reading the text. STE stands for self trapped exciton and the symbols are defined throughout the text.

2 Experimental

$PbWO_4$:Tb^{3+} powders were prepared by a solid state synthesis of 8 hours at 800°C in air with $PbNO_3$ (Pro Analyse) and WO_3 (Alfa Aesar, 99.8%) as precursors. Tb was added in the form of TbF_3 (Alfa Aesar, 99.9%). The same molar concentration of NaF (Alfa Aesar) was added for

(partial) charge compensation. Phase purity of the obtained powders was verified through X-ray diffraction (XRD) on a Siemens D5000 diffractometer (40 kV, 40 mA) using CuKα_1 radiation and comparison of the obtained XRD pattern with ICSD No. 16189 [33].

Steady state photoluminescence emission and excitation spectra were measured with an Edinburgh FS920 fluorescence spectrometer while time-resolved measurements were performed with an intensified CCD (Andor iStar DH720), combined with Jarrel-Ash monochromator upon pulsed nitrogen laser excitation (λ_{exc} = 337 nm, pulse <1 ns) and if desired combined with a dye laser module (λ_{exc} = 380 nm).
Diffuse reflectance spectoscopy was performed with a Varian Cary 500 spectrophotometer, equipped with an internal 110 mm $BaSO_4$ - coated integrating sphere.

Temperature dependent measurements were performed by putting the powders inside a crysotat (Oxford Instruments Optistat CF), with temperature range from 4.2 K to 475 K.

3 Results

3.1 Diffuse reflectance spectroscopy

From the diffuse reflectance spectra, the Kubelka-Munk spectra were calculated (see Fig. 2) and a value of 3.87 ± 0.10 eV was found for the optical band gap [34]. The electronic band gap is then estimated to be 4.18 ± 0.25 eV upon using the empirical proportionality factor of 1.08 [35, 36]. Though this factor was obtained with a rather low accuracy from self-trapped exciton energies in binary halides, it is frequently used for hosts of different composition [37]. Absorption bands of intrinsic defects are known to be present at energies around the fundamental absorption offset, but the concentration of defects is assumed to be sufficiently low to rely on the above optical band gap value.

Doping with Tb does not significantly change the shape of the diffuse reflectance spectra, however for 5% Tb^{3+} the abosprtion edge appears to shift. Nikl *et al.* explained this in the case of $PbWO_4$: Pr^{3+} by a charge transfer transition from oxygen to the dopant, or to a type of charge transfer between oxygen ligands and WO_4^{2-} - RE centres, however they observed a larger shift than the one observed here. Kobayashi *et al.* ascribed this to a perturbation induced by the introduction of dopants [26, 38]. The spectra of $PbWO_4$: 1% Tb^{3+} and 5% Tb^{3+} show no strong Tb 4f-4f absorption due to the low absorption cross-section of these transitions. In addition, two extra bands around 425 nm and 350 nm can be observed for these materials, possible related to new defects.

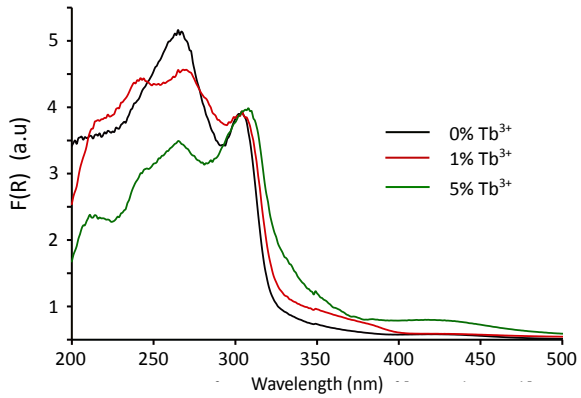

Figure 2: Kubelka-Munk spectra for the undoped, 1% Tb^{3+} and 5% Tb^{3+} sample.

3.2 Luminescence excitation and emission spectra

Luminescence excitation and emission spectra were measured at low temperature to reduce the thermal effects. At 10 K, excitation at 270 nm in undoped $PbWO_4$ results in a blue emission band peaking at 420 nm whereas excitation at 340 nm gives rise to an emission band with maximum intensity at 530 nm (Fig 3, right). The excitation spectrum of both (monitored at $\lambda_{em} = 400$ nm and 575 nm) is illustrated in Fig 3 on the left. The emission wavelengths are chosen in order to minimize the contribution of the respectively green and blue emission band. The blue emission is generally ascribed to emission of the WO_4^{2-} complex [39] and its excitation spectrum peaking at 270 nm indeed coincides roughly with the diffuse reflectance spectrum of the undoped $PbWO_4$. The centre has a nearly tetrahedral site symmetry, with the lowest lying excited states being the two almost degenerate triplet levels $^3T_1$ and $^3T_2$. Excitation takes place from the $^1A_1$ ground state to the singlet states $^1T_1$ and $^1T_2$ whereas luminescence arises from the spin forbidden $^3T_1 \rightarrow {}^1A_1$ transition [30, 40]. Annenkov *et al.* located the transition to the singlet states at 275 nm and to the triplet state at 325 nm [30]. The green emission on the other hand is associated with a transition in a centre with an oxygen ion vacancy and its excitation spectrum exhibits an extra band at 340 nm, which is absent in the diffuse reflectance spectrum. Probably, the contribution of these defect centres in the total spectrum is there too low to be observed. At 310 nm an extra peak can be observed, which also appears in the excitation spectrum of the blue host emission at higher temperatures.

The emission spectrum at room temperature and the excitation spectra at 10 K of the Tb^{3+} doped samples (1% Tb^{3+} and 5% Tb^{3+}) for the emission from the $^5D_3$ (left, $\lambda_{em} = 435$ nm) and $^5D_4$ (right, $\lambda_{em} = 545$ nm) level are shown in Fig 4. The band gap absorption is clearly present in both spectra, but the absorption band attributed to the defect centres situated around 340 nm can only be detected in the excitation spectrum of the $^5D_4$ emission and is more prominent for high Tb^{3+} concentrations. After excitation in the defect centres the energy transfer to the Tb^{3+} ions apparently skips the $^5D_3$ level. No extra bands as compared to the excitation spectrum of the host emission are found. At lower energies the characteristic $4f^8$-$4f^8$ transitions of Tb^{3+} are present.

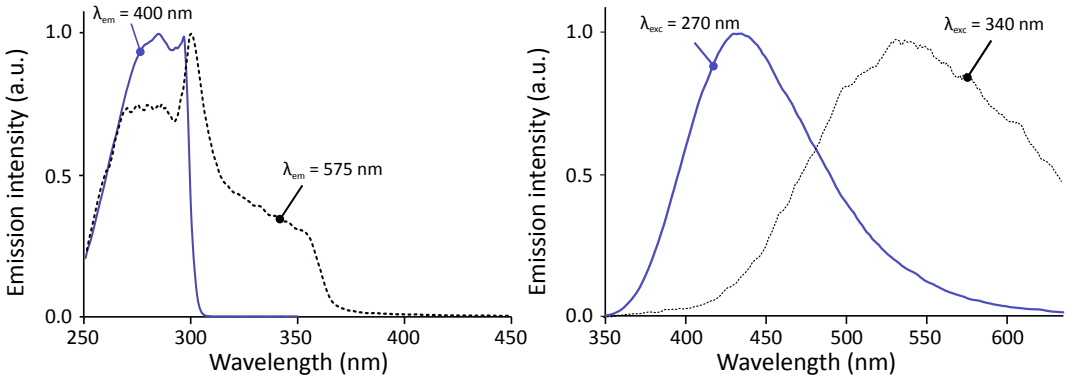

Figure 3: Left: Excitation spectra of the blue host (solid blue line, $\lambda_{em} = 400$ nm) and green defect (dotted black line, $\lambda_{em} = 575$ nm) emission bands of undoped $PbWO_4$, measured at 10 K. Right: Spectra of the blue host (solid blue line) and green defect (dotted black line) emission bands of undoped $PbWO_4$ upon excitation at respectively $\lambda_{ex} = 270$ nm and 340 nm at 10 K.

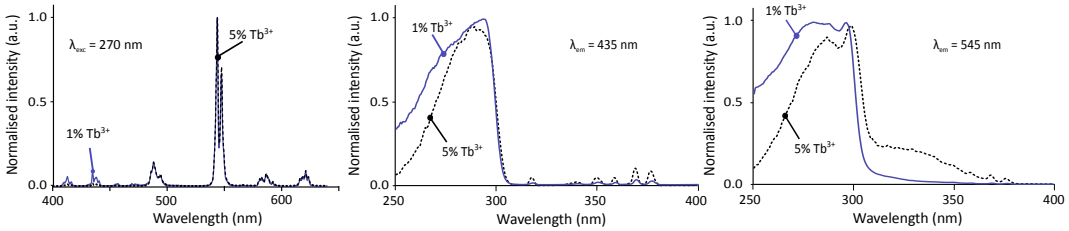

Figure 4: Left: Emission spectrum ($\lambda_{exc} = 270\,\text{nm}$) of the Tb-doped $PbWO_4$ samples (1% and 5% Tb^{3+}) at room temperature. Middle: Excitation spectra of the Tb^{3+} $^5D_3$ emission in $PbWO_4$ for different Tb^{3+} concentrations ($\lambda_{em} = 435\,\text{nm}$). Measured at 10 K. Right: Excitation spectra of the Tb^{3+} $^5D_4$ emission in $PbWO_4$ for different Tb^{3+} concentrations ($\lambda_{em} = 545\,\text{nm}$) at 10 K.

In Figure 5 the emission spectrum upon excitation at different wavelengths is shown at 10 K. Excitation in both WO_4^{2-} ($\lambda_{\text{exc}} = 270\,\text{nm}$) and WO_3 ($\lambda_{exc} = 340\,\text{nm}$) centres results in their respective intrinsic emission, which is now only visible as a weak background, together with $^5D_3$ and $^5D_4$ emission from the Tb^{3+} ion. Apparently the energy transfer from the host to the Tb^{3+} ions is not complete especially for the low Tb^{3+} concentrations. Direct excitation of the defect centres indeed lacks $^5D_3$ emission.

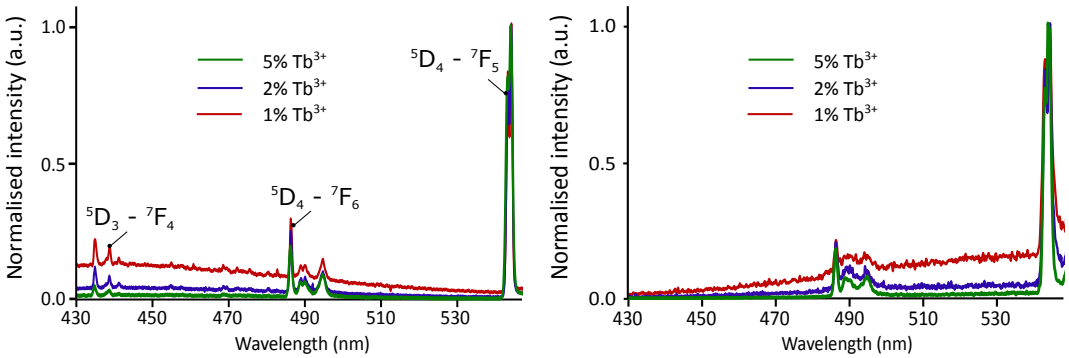

Figure 5: Emission spectra ($\lambda_{exc} = 270\,\text{nm}$ (left) and $\lambda_{exc} = 340\,\text{nm}$ (right)) of the Tb-doped samples at 10 K.

Zooming in on the $^5D_4$-$^7F_5$ transition ($\lambda_{em} = 545\,\text{nm}$) of Tb^{3+}, some significant spectral differences are found upon excitation at different wavelengths (Fig. 6). Excitation of the defect centres ($\lambda_{exc} = 340\,\text{nm}$) results in an asymmetric broadening of the two most prominent peaks as compared to excitation across the band gap ($\lambda_{exc} = 270\,\text{nm}$). The first peak broadens towards shorter wavelengths, the second one to longer wavelengths and this spread of the energy levels must be the consequence of a larger crystal field felt by the Tb^{3+} ions. For excitation at 270 nm and 340 nm apparently two different sites for the Tb^{3+} ions are addressed, which is often referred to as site selective excitation. Direct excitation to the $^5D_3$ level of Tb^{3+} ($\lambda_{exc} = 378\,\text{nm}$) results in a superposition/combination of the two spectra and both types of Tb^{3+} ions are apparently excited. The above description is valid for the 5% Tb^{3+} sample, for the other Tb^{3+} concentrations the superposition is far less explicit (Fig 6, right). Apparently the Tb^{3+} ions show a preferential occupation for the normal sites and only when the concentration is large enough, the Tb^{3+} ions occupy sites near defect centres.

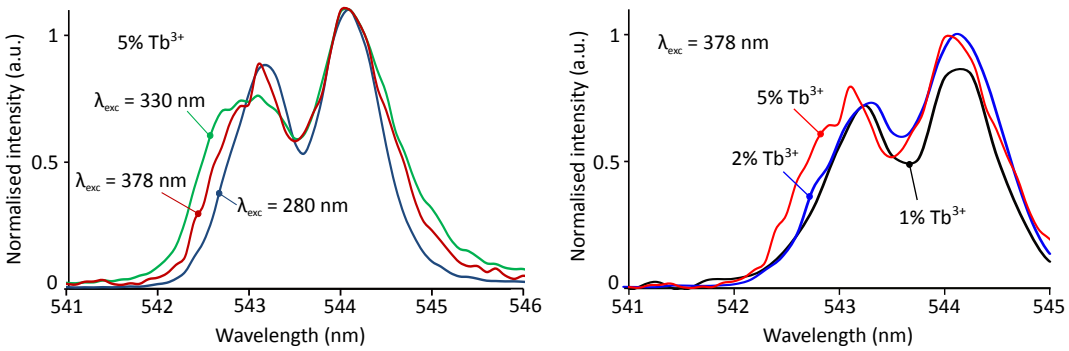

Figure 6: Left: $^5D_4$-$^7F_5$ transition of Tb^{3+} upon excitation at 270 nm, 330 nm and 378 nm at 10 K for $PbWO_4$: 5% Tb^{3+}. Right:$^5D_4$-$^7F_5$ transition of Tb^{3+} upon excitation at 378 nm at 10 K for $PbWO_4$: 1%, 2% and 5% Tb^{3+}.

3.3 Thermal quenching of host and Tb^{3+} emission

First, the thermal quenching of the host emission of undoped $PbWO_4$ is investigated, discriminating between excitation across the band gap (λ_{exc} = 270 nm) and excitation of the defect centres (λ_{exc}= 340 nm). Second, the intensity of both the host and Tb^{3+} emission is investigated for $PbWO_4$: Tb^{3+} in a temperature range from 75 K to 475 K for three cases: excitation across the band gap, of defect centres and, only for the Tb^{3+} emission, to the Tb^{3+} levels. This direct excitation can be analysed both by thermal quenching and by the temperature dependent decay characteristics of the emission.

The investigated characteristics of the Tb^{3+} emission are only dependent on the emitting ^5D_J energy level and not on the final ^7F_J level, therefore one transition for each energy level is taken as representative for all the emission coming from the respective energy levels. The obtained data points in the thermal quenching profiles correspond to the integrated intensities of the $^5D_3$ - $^7F_4$ (432 to 442 nm) and $^5D_4$ - $^7F_5$ (535 to 555 nm) transition.

The solid lines are the the fits of the solutions of the rate equations of section 4 and their meaning will become clear in that section.

3.3.1 Undoped $PbWO_4$

For the undoped samples, excitation over the band gap (λ_{exc} = 270 nm) results in a constant emission intensity (λ_{peak} = 420 nm) up to 175 K after which the intensity drops dramatically (Fig 7, left). Between 175 K and room temperature, the emission spectrum shifts to longer wavelengths (not shown) pointing to an increased contribution of defect emission in the total spectrum.

Direct excitation of the defect centres (λ_{exc} = 340 nm) shows thermal quenching of the green emission from 75 K on. No temperature dependent shift in the emission spectrum is observed for this excitation wavelength (Fig 7, right).

For both blue host and green defect emission, the absorption band associated with the band gap shows a broadening towards longer wavelengths upon increasing temperature (not shown).

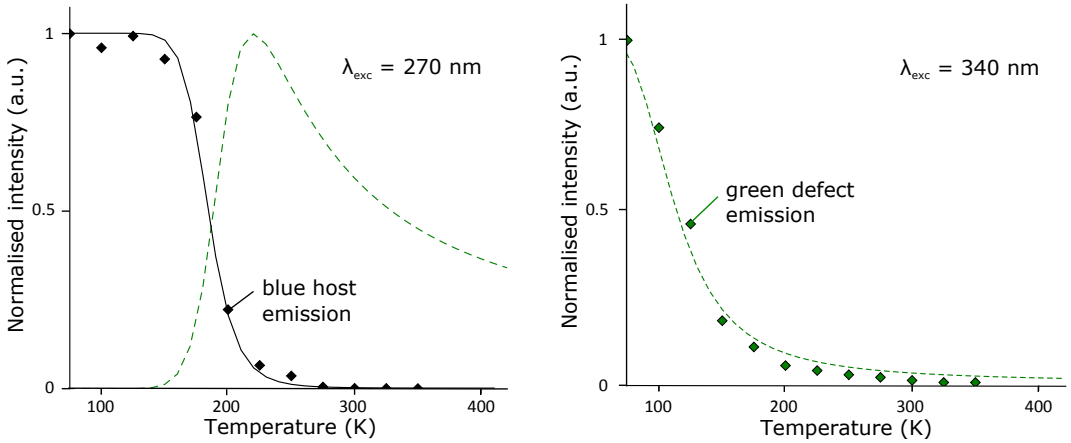

Figure 7: Left: Thermal quenching of the host emission upon band gap excitation (λ_{exc} = 270 nm). The diamonds are the integrated intensities ($\lambda_{em} = 350 - 420$ nm). The solid lines are the solutions of Eq. 2a (solid black line) and Eq. 2b (dashed green line). Right: Thermal quenching of the green defect emission (λ_{exc} = 340 nm). The diamonds are the integrated intensities, the solid line is the fit of the solution of Eq. 2b.

3.3.2 $PbWO_4$: Tb^{3+}

Comparing these profiles with the Tb^{3+} doped samples is indicative for the influence of the Tb^{3+} doping on the excited state dependencies. No subsequent energy transfer processes are expected to occur.

- **Excitation at 270 nm**

The quenching profile of the host emission after excitation across the band gap (Fig. 8, black circles) shows two main differences compared to the undoped samples. Firstly, the decrease in intensity starts at a lower temperature, 125 K instead of 175 K and secondly, the decline of the decrease is less extreme. Both are probably related to the extra energy transfer path towards the Tb^{3+} ion.

The thermal quenching profile of the $^5D_4$ emission (Fig. 8, green squares) can be subdivided in three parts irrespective of the Tb^{3+} concentration. Between 75 K and 125 K the emission remains more or less constant, after which the intensity starts to increase to reach its maximum at 175 K. Going to higher temperatures results in a decrease of the emission intensity. The concentration dependence manifests itself in the difference in intensity at 75 K with respect to the intensity at 175 K. The higher the Tb^{3+} concentration, the higher this initial relative intensity. At 125 K, when the host emission starts to decrease (black circles), the Tb^{3+} emission starts to increase. The decrease of the Tb^{3+} emission, starting from 175 K coincides with the decrease of the host emission of pure $PbWO_4$ (Fig. 7, left).

The thermal quenching behaviour of the $^5D_3$ and $^5D_4$ emission (Fig 8, blue diamonds) is comparable, only the relative emission intensity of the $^5D_3$ emission at 75 K is higher with respect to the emission from $^5D_4$.

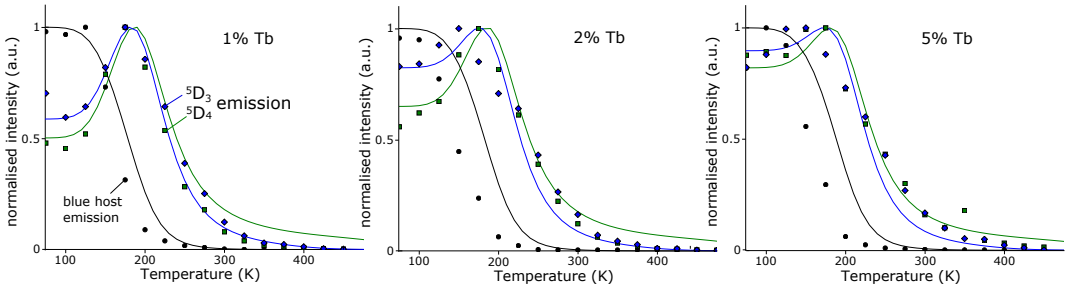

Figure 8: Thermal quenching of the blue host emission (black), $^5D_3$ emission (blue) and $^5D_4$ emission (green) of $PbWO_4$:Tb^{3+} (1%, 2% and 5%) upon excitation at 270 nm. The symbols are the integrated emission intensities, the solid lines are the solution of Eq. 4.

- **Excitation at 340 nm**

The green defect emission, excited at 340 nm shows immediate quenching from 75 K (Fig. 9).

The quenching profile of the emission coming from the $^5D_4$ level is the same for all Tb^{3+} concentrations and comparable with the profile of the defect emission itself. No temperature dependent energy transfer process occurs between the defect centres and the Tb ions. Note that the $^5D_3$ level cannot be populated by excitation at this wavelength in the investigated temperature range.

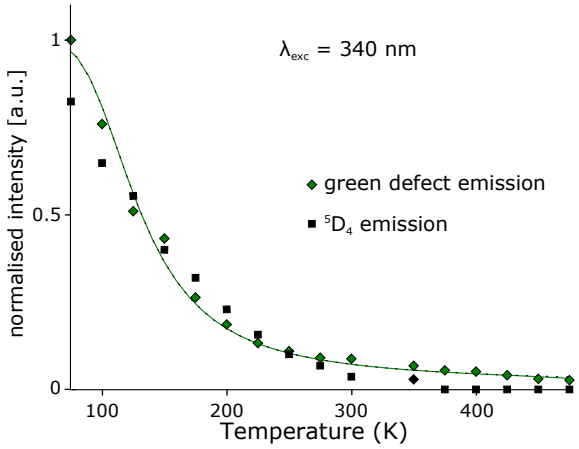

Figure 9: Thermal quenching of the green defect emission (black) and Tb^{3+} $^5D_4$ emission (green) of $PbWO_4$:Tb^{3+} (5%) upon excitation at 340 nm. The symbols are the integrated emission intensities, the solid lines are the solution of Eq. 4

- **Excitation to a ^5D_J level of Tb^{3+}**

Upon direct excitation of the $^5D_3$ level of Tb^{3+}, both $^5D_3$ and $^5D_4$ emission is observed. The decay profiles of the $^5D_3$ emission are shown in Fig. 11 (left), recorded at 75 K upon excitation at 380 nm. This decay is not mono-exponential and the deviation from a single exponential becomes more significant for increasing Tb^{3+} concentration. Furthermore, a build - up in the intensity of the $^5D_4$ emission is observed during the first few microseconds (Fig. 11, right). In Fig. 10 the emission spectra at 75 K upon excitation to the $^5D_3$ level are shown and a decreasing fraction of $^5D_3$ emission relative to $^5D_4$ emission is observed for increasing Tb^{3+} concentration. The decay profiles as well as the emission spectra proves the existence of a cross-relaxation process between the two emitting energy levels.

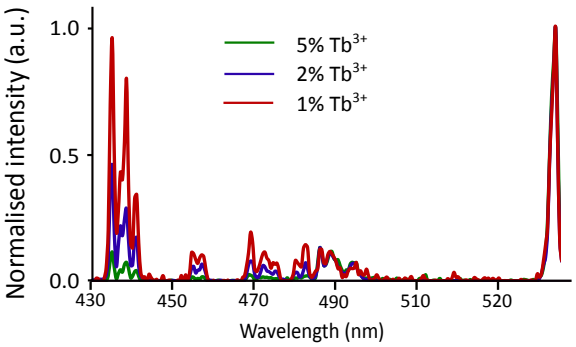

Figure 10: Emission spectrum (λ_{exc} = 377 nm) normalised to the peak of the $^5D_4$-$^7F_5$ transition at 75 K.

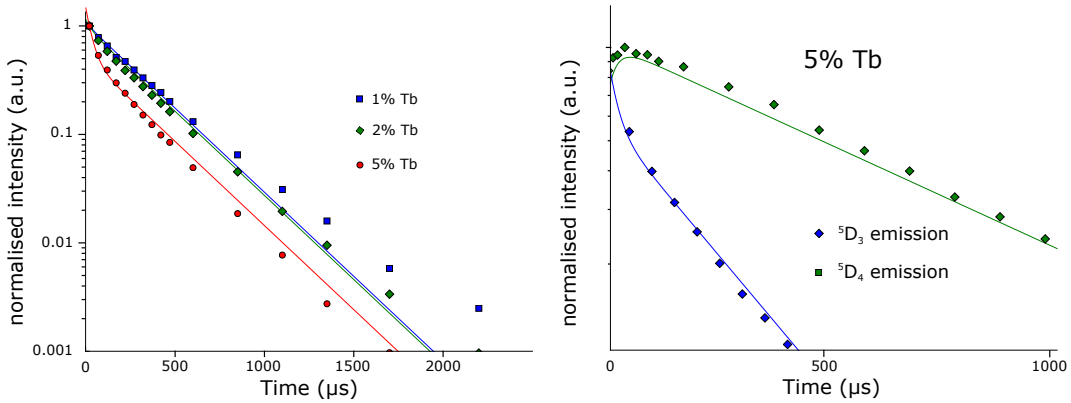

Figure 11: Right: decay profiles of the $^5D_3$ emission of $PbWO_4$: 1%, 2% and 5% Tb^{3+} at 75 K (λ_{exc} = 377 nm). Left: a zoom on the first microseconds of the $^5D_4$ and $^5D_3$ emission.

The temperature dependence of the emission efficiency of the $^5D_3$ level manifests itself by the decay profiles and steady state spectra. From Fig. 12 (left) it can be seen that the intensity of the $^5D_3$ emission remains more or less constant up to room temperature after which the decrease sets in. The emission from the $^5D_4$ level follows the same trend pointing to a temperature independent cross-relaxation process. This quenching behavior is encountered for the decay profiles as well. Indeed in Fig. 12 (middle and right), the decay of the $^5D_3$ emission (1% Tb^{3+}) is depicted at 75 K and 350 K. Independent of the Tb concentration, the decay starts to fasten from room temperature onwards. The large spread on the data points should be no surprise for excitation to a 4f-level of a lanthanide as fluctuations in the absorption strength occur due to thermally induced excitation towards higher lying crystal field levels of the $^7F_6$ multiplet and the broadening of the absorption lines. In addition, the low absorption efficiency of this energy level, as can be seen form the excitation spectra (Fig. 4), induces relatively large experimental errors.

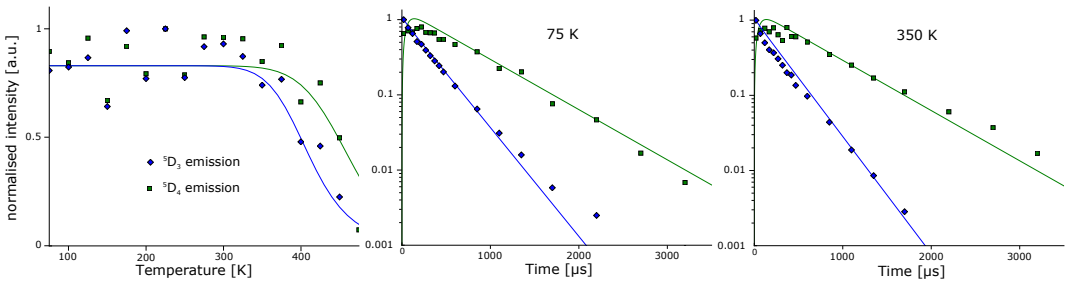

Figure 12: Left:Thermal quenching of the $^5D_3$ (blue) emission and $^5D_4$ (green) emission of $PbWO_4$: Tb^{3+} (1%, 2% and 5%) upon excitation at 378 nm. Middle and right : Decay profiles of the $^5D_3$ (blue) and $^5D_4$ (green) emission at 75 K (middle) and 350 K (right). The diamonds ($^5D_3$) and squares ($^5D_4$) are the integrated emission intensities, the solid lines are the solutions of Eq. 5.

Determining the efficiency of the emission from the $^5D_4$ level is even less straightforward. The low absorption strength of the $^5D_4$ level excludes direct excitation to this level, making thermal quenching profiles obtained from steady spectra not convenient to investigate the efficiency. Therefore, only the temperature dependence of the decay profiles is used for evaluation. These profiles are shown in Fig 13 (left) for different Tb^{3+} concentrations at 75 K ($\lambda_{exc} = 337$ nm). At 75 K, the decay profiles are characterized by two exponential contributions, with decay constants of 0.63 ms and 65 ms. The fraction of this component is only 2% of the total decay and thus negligble for the discussion. For 1% Tb^{3+} the slow component is already disappeared at 250 K whereas for 5% Tb^{3+} it is observed until 350 K. The decay profiles at 475 K are shown in Fig 13 (right). The main decay component of the $^5D_4$ emission remains stable for all Tb^{3+} concentrations with varying temperature, only from 400 K on, a slight decrease sets in. These lifetimes correspond well with the typical values found in literature for Tb^{3+} doped scheelites [41, 42].

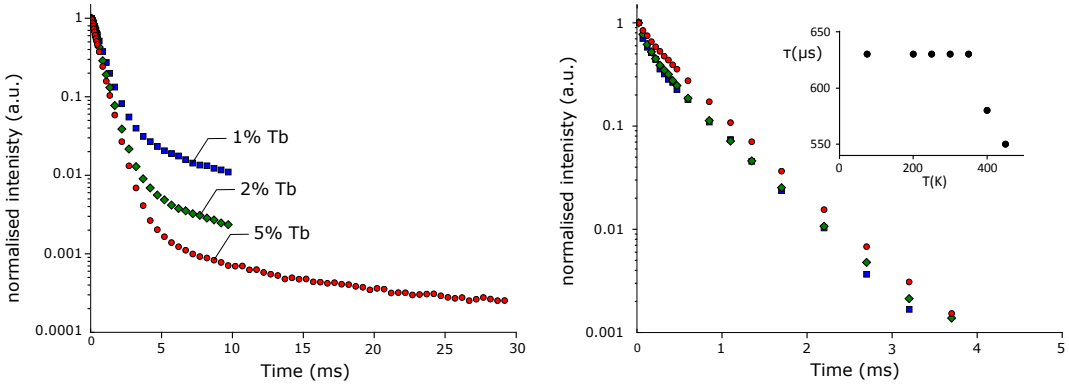

Figure 13: Decay profiles of the $^5D_4$ emission at 75 K (left) and 475 K (right) upon excitation at 337 nm.

4 Discussion

The above results indicate that multiple factors influence the quenching of a luminescent centre. Depending on the excitation wavelength and the type of sample, different temperature dependences are found for the same luminescent transitions. In the following, an attempt is made to point out the involved mechanisms between the host-related centres, between the host-related centres and the Tb ions and between the Tb ions themselves. All these processes are introduced in rate equations for the involved energy levels. The fit of these equations to the experimental data will give both a quantitative and qualitative indication of the different processes.

4.1 Host related excitation

Tb^{3+} emission upon excitation in host related features points unarguably to an energy transfer process between host and impurity ions. The thermal quenching profiles can at least partly reveal the transfer channels between both. As already mentioned, in lead tungstate without intentional doping, luminescence occurs mainly due to transitions in WO_4^{2-} centres. The transitions take place from one of the 2p oxygen shells to the empty 5d shell of W^{6+}. The break up of the closed shell condition by this valence excitation involves a considerable lattice relaxation. This strong electron - lattice coupling makes trapping of the electronic excitation possible, resulting in a self-trapped exciton (STE) which will largely influence the luminescence and energy transfer properties of the material [32, 39, 43, 44].

Taking this self-trapped exciton into account, the observed thermal quenching in the undoped sample can be explained as follows. Excitation at 270 nm results in a number of self-trapped excitons which can decay radiatively with a certain decay rate τ_h observed as the blue host emission peaking at 440 nm. If temperature is sufficiently high, the available thermal energy can equal the activation energy of the exciton, allowing energy migration through the crystal. The diffusion of these excitons is a multistep energy transfer process and the energy can reach activator ions or defects in the material. These activators and/or defects can at their turn emit light, or for some specific types of defects decay non - radiatively and thus quench the luminescence. In this way, Tb ions can be considered as activators and will be discussed later. One of the possible defects are the WO_3 centres causing the green defect emission peaking at 550 nm [45]. The temperature dependence of the migration process is incorporated in the diffusion constant D:

$$D = D_0 \exp\left(-\frac{\Delta E}{kT}\right) \tag{1}$$

Next to this excitation across the optical band gap, direct excitation of the defect centres is considered as well. The observed quenching and absence of a shift in the emission spectrum points to quenching due to photoionization through the conduction band without transfer to the WO_4^{2-} centres. In order to formulate the rate equations, it is sufficient to consider two host-related states. The first one represents the triplet state of the WO_4^{2-} centre responsible for the blue host emission with population N_h, corresponding to the number of excited ions and the second one refers to the ^2E level of WO_3, being responsible for the observed green emission with a population N_d. It is assumed that there are sufficient centres and mobility so no saturation effects will take place. The rate equations for the population of both can be written as follows:

$$\frac{dN_h}{dt} = \mathrm{pump_h} - N_h\left[\Gamma_0 \exp\left(-\Delta E_h/kT\right) + \Gamma_h\right] \tag{2a}$$

$$\frac{dN_d}{dt} = \mathrm{pump_d} + N_h\Gamma_0 \exp\left(-\Delta E_h/kT\right) + N_d\left[\Gamma_d - \Gamma_{0d} \exp\left(-\Delta E_d/kT\right)\right] \tag{2b}$$

with the rates $\Gamma_h = 10^6\,\mathrm{s}^{-1}$ and $\Gamma_d = 10^5\,\mathrm{s}^{-1}$ derived from the decay profiles at low temperature [18]. Excitation into a certain energy level x, is written as $\mathrm{pump_x} \neq 0$. Fitting the solution of equation 2 for excitation in the band gap ($\mathrm{pump_h} \neq 0$; $\mathrm{pump_d} = 0$) to the thermal quenching data, results in an escape frequency $\Gamma_0 = 10^{14}\,\mathrm{s}^{-1}$ and $\Delta E_h = 0.26\,\mathrm{eV}$ (Fig. 7). This 0.26 eV is the thermal energy needed to release the self-trapped exciton and allow energy migration. From Fig. 7 it can be seen that upon increasing temperature, the defect WO_3 centres (dashed green line) get populated. The measured emission at this excitation wavelength and temperature is a combination of both the intrinsic WO_4^{2-} emission (solid black line) and the defect emission (dashed green line). Indeed, this corresponds with the observed shift to longer wavelengths of the emission band at increasing temperature.

Direct excitation of the defect centres (Fig. 7, $\mathrm{pump_h} = 0$; $\mathrm{pump_d} \neq 0$) results in a $\Delta E_d = 0.05\,\mathrm{eV}$ however with a much slower frequency factor $\Gamma_{0d} = 10^9\,\mathrm{s}^{-1}$. The value of ΔE_d positions

the emitting energy level of the defect centre with respect to the conduction band with the assumption that photoionization is responsible for thermal quenching.

Doping this material with Tb^{3+} results in additional energy transfer channels (Fig. 8). At first, direct energy transfer from the self-trapped excitons to the Tb^{3+} activator ions is possible. This single step energy transfer process can be the result of multipole-multipole interaction or exchange interaction. The electromagnetic multipole interaction was first described by Förster and Dexter for dipole-dipole interaction and later extended to higher order terms [46, 47]. For both types of interaction, the transfer rate between a sensitizer, here the exciton, and the activator, here the Tb^{3+} ions, is given by following expression:

$$\omega_{S^*A} = \frac{2\pi}{\hbar} |\langle S, A^* | \hat{\mathcal{H}}_{int} | S^*, A \rangle|^2 \int g_S(E) g_A(E) \mathrm{d}E \tag{3}$$

with $\hat{\mathcal{H}}_{int}$ the hamiltonian specifying the interaction between the initial and final state and the integral the spectral overlap between both. The temperature dependence of the transfer process is limited to the temperature dependence of this spectral overlap and thus quasi negligible. On the other hand, a large concentration dependence will arise due to the distance dependence of $\hat{\mathcal{H}}_{int}$. For multipole interactions an $(\frac{1}{R})^n$ dependence can be found for the transfer rate, with n depending on the dominant multipole moment, whereas exchange interaction shows an $exp(1-R)$ dependence [48]. In both cases, the transfer rate should increase with increasing Tb^{3+} concentration. The transfer rate from the host to the $^5D_4$ and $^5D_3$ level is hereafter referred to $\Gamma(C_{h4})$ and $\Gamma(C_{h3})$ respectively.

Apart from this direct energy transfer contribution, a temperature dependent energy transfer process will take place if the exciton has received enough thermal energy to undergo energy migration to the Tb^{3+} ions. This process will occur with a certain transfer rate Γ_{h-Tb} and activation energy ΔE_{h-Tb}. Of course the transfer mechanisms as described for the undoped samples remain valid and should still be considered.

In addition to this host-sensitized energy transfer, energy transfer from the defect centres to the Tb^{3+} ions should be taken into account (Fig. 9). From Fig 4 it is clear that the efficiency of the energy transfer from defects to Tb^{3+} is concentration dependent. The higher the Tb^{3+} concentration, the larger the contribution is of the excitation via the defect centres in the excitation spectrum. Based on the thermal quenching data (Fig. 9) no temperature dependence in the transfer rate is expected as the emission from the Tb^{3+} ions follows the quenching profile of the green defect emission in the whole investigated temperature range. Therefore, energy transfer occurs probably via a direct energy transfer process as described above. The specific character of this process is again difficult to determine. The lack of $^5D_3$ emission is owing to the too limited spectral overlap between both levels.

The rate equations of Eq. 2 should now be extended with the $^5D_3$ level, with population N_3 and the $^5D_4$ level, with population N_4 and the above described transfer mechanisms between host and Tb^{3+} ions. Based on these rate equations it becomes clear that a decreasing intensity of the host emission should not solely be linked to quenching and thus a loss in energy but also to the feeding of other energy levels, including defect emisison and Tb^{3+} ions:

$$\begin{aligned}\frac{dN_h}{dt} &= \mathrm{pump_h} \\ &\quad - N_h \left[\Gamma_0 \exp\left(-\Delta E_h/kT\right) + \Gamma_{h-Tb} \exp\left(-\Delta E_{h-Tb}/kT\right) + \Gamma_h + \Gamma(C_{h4}) + \Gamma(C_{h3})\right] \quad (4a)\end{aligned}$$

$$\frac{dN_d}{dt} = \mathrm{pump_d} + N_h \times \Gamma_0 \exp\left(-\Delta E_h/kT\right) - N_d \left[\Gamma_{0d} \exp\left(-\Delta E_d/kT\right) + \Gamma(C_{d4}) + \Gamma_d\right] \quad (4b)$$

$$\begin{aligned}\frac{dN_4}{dt} &= \mathrm{pump_4} + N_h \left[\Gamma_{h-Tb} \exp\left(-\Delta E_{h-Tb}/kT\right) + \Gamma(C_{h4})\right] + N_d \times \Gamma(C_{d4}) \\ &\quad - N_4 \left[\Gamma_{0-Tb} \exp\left(-\Delta E_{X4}/kT\right) + \Gamma_4\right] \quad (4c)\end{aligned}$$

$$\frac{dN_3}{dt} = \text{pump}_3 + N_h \left[\Gamma_{h-Tb} \exp\left(-\Delta E_{h-Tb}/kT\right) + \Gamma(C_{h3})\right] - N_3 \left[\Gamma_{0-Tb} \exp\left(-\Delta E_{X3}/kT\right) + \Gamma_3\right] \quad (4d)$$

The solutions of equation 4 are fitted to the experimental data described in section 3 simultaneously for the different excitation mechanisms and Tb^{3+} concentrations. In this way, a complete picture of the system can be obtained. As can be seen in Fig. 8 for the situation upon excitation of the WO_4^{2-} centres ($\lambda_{exc} = 270\,\text{nm}$; $\text{pump}_h \neq 0$), there is a nice correlation between the experimental data and the fit, especially for the 1% Tb^{3+} case. There is no doubt that the fits for the 2% Tb^{3+} and 5% Tb^{3+} samples can be improved by separately adjusting the values of the different parameters, however this would lead to over-parametrization of the fits which is unfavourable.

The obtained values for the different rates and energies are listed in Table 1 and the decay rates Γ_4 and Γ_3 are derived from the fits of the decay profiles obtained in section 4.2. The emission intensity at 75 K can thus be linked to a direct energy transfer to the Tb^{3+} ions. Upon increasing temperature, the remaining trapped excitons are released and can reach the non-excited Tb ions. If temperature is high enough, these excitons are able to reach the quenching defects and competition between transfer to Tb ions and transfer to quenching centres starts. Due to the faster transfer rate of the latter, the population of the Tb ions via host excitation becomes increasingly rare and their emission quenches. The escape frequency is somewhat higher than for the undoped material(5.10^{14} instead of 10^{14} Hz), but the thermal quenching energy ΔE_h = 0.26 eV remains the same. It may be surprising that at these high Tb concentration the transfer to quenching centres still dominates over the transfer to Tb^{3+} ions. Therefore, as an alternative, thermal quenching in the WO_4 centre itself could be proposed instead of transfer to other centres in the material. As both are described by the same differential equation, this different interpretation would not lead to other values of energy barriers or transfer rates.
The lower temperature for the start of the quenching of the host emission - 125 K for the doped samples as compared to 175 K for the undoped samples - is thus indeed the result of the extra transfer channel towards the Tb^{3+} ions.

The thermal quenching of the $^5D_3$ and $^5D_4$ emission itself is also incorporated in Eq. 4 via the contribution of $N_J \times \Gamma_{0-Tb} \exp(-\Delta E_{XJ}/kT)$. Comparing the temperature dependence of the emission coming from the ^5D_J level after excitation in host-related energy levels (Fig 8) and after direct excitation (Fig. 12, left), it can readily be deduced that the quenching upon host excitation sets in at a lower temperature than quenching upon direct excitation. From the above analysis it is clear that the quenching of the ^5D_J emission in the case of host excitation is the consequence of a decreasing excitation efficiency of the Tb^{3+} energy levels and not of a decreasing emission efficiency. As such, only a lower limit for ΔE_{XJ} can be deduced from the quenching profiles upon host excitation and the actual value will be determined in section 4.2.

The transfer rates for direct energy transfer, $\Gamma(C_{hJ})$, indeed increase gradually with increasing Tb concentration. The discrepancy between $\Gamma(C_{h3})$ and $\Gamma(C_{h4})$ can stem from the difference in spectral overlap, which is higher for the $^5D_3$ level compared to the $^5D_4$ level.

4.2 Direct excitation of the energy levels of Tb^{3+}

To consider the thermal quenching of the $^5D_4$ and $^5D_3$ emission after excitation to the $^5D_3$ level both thermal quenching and decay profiles are taken into account (Fig. 12). As stated above, coupling between the two terbium levels occurs via a cross-relaxation process. The higher the Tb^{3+} concentration, the higher the number of ions involved in this cross-relaxation process (Fig. 10). These coupled ions can after excitation to the $^5D_3$ level give rise to emission from the $^5D_4$ level. By contrast, the uncoupled ions show emission only from the $^5D_3$ level. Therefore, a distinction is now made between coupled ions with population N_{Jc}, exhibiting cross-relaxation

and uncoupled ions, N_J. The total $^5D_4$ and $^5D_3$ emission is the weighted sum of the uncoupled and coupled situation, with a weight factor of respectively N_{iso} and (1-N_{iso}).

The rate equations are now given by:

$$\frac{dN_{4c}}{dt} = \text{pump}_4 + N_{3c} \times \Gamma_c - N_4 \times \Gamma_{0-Tb}\left[exp\left(-\Delta E_{X4}/kT\right)\right] - N_4 \times \Gamma_4 \tag{5a}$$

$$\frac{dN_4}{dt} = \text{pump}_4 - N_4 \times \Gamma_{0-Tb}\left[exp\left(-\Delta E_{X4}/kT\right)\right] - N_4 \times \Gamma_4 \tag{5b}$$

$$\frac{dN_{3c}}{dt} = \text{pump}_3 - N_{3c} \times \Gamma_{0-Tb}\left[exp\left(-\Delta E_{X3}/kT\right)\right] - N_{3c} \times \Gamma_c \tag{5c}$$

$$\frac{dN_3}{dt} = \text{pump}_3 - N_3 \times \Gamma_{0-Tb}\left[exp\left(-\Delta E_{X3}/kT\right)\right] - N_3 \times \Gamma_3 \tag{5d}$$

In Fig. 12, the situation upon excitation to the $^5D_3$ level ($\lambda_{exc} = 378\,\text{nm}$, $\text{pump}_3 \neq 0$) is shown for $PbWO_4$: 1% Tb^{3+}. The solid lines again correspond to the fit of the solutions of Eq. 5 and match very closely with the experimental data. The obtained values for Γ_0, Γ_3, Γ_4, ΔE_{4X} and ΔE_{3X} can be found in Table 1.
The *quenching energy* of the $^5D_3$ level, $\Delta E_{X3} = 0.51\,\text{eV}$, is confirmed both by the thermal quenching profiles of the emission and by the temperature dependence of the decay profiles. The exact nature of the quenching of 4f-4f emission is not known and possible explanations are multiphonon relaxation processes, back transfer to for instance the WO_4^{2-} centres or via the IVCT. In Fig 12, the decay profiles of both energy levels are shown at different temperatures for the situation with 5% Tb doping. In this situation the fraction of coupled ions is apparently 65 % and the cross-relaxation occurs with an transfer rate of $5.10^6\,\text{s}^{-1}$. The decay profiles of the $^5D_4$ emission (Fig. 13) are reproduced by a thermal quenching energy of 0.66 eV for all three concentrations.

The found energy differences are displayed in a conceptual total energy level diagram, displayed in Fig. 1. Herein, three distinct configurational coordinate diagrams are shown for respectively WO_4^{2-}, WO_3 and Tb^{3+} centres. In these diagrams, the ordinate represents the total energy of the complete system, containing the electrons that are allocated to the defect as well as all other electrons of the compound. For this reason, it has no meaning to add concepts such as valence or conduction bands to the energy level diagram because they correspond with the energy levels of single particle orbitals [37]. Thermal quenching and temperature dependent energy transfer channels are represented through additional energy surfaces which are at some point resonant with the initial and final many-body state. From this diagram, it is clear that vibronic interactions cannot be neglected in a correct description of luminescence centres. The curvature of the energy surfaces in configurational coordinate space ensures that the fixed energy difference between the $^5D_4$ and $^5D_3$ multiplets of 0.72 eV is not reflected in their thermal quenching energy difference of 0.15 eV. Notwithstanding the values of Γ_0 are related to the curvature, which is in reality a highly dimensional tensor, the exact relation between both is unknown and the absolute numbers of the curvature are inaccessible from modelling through rate equations.

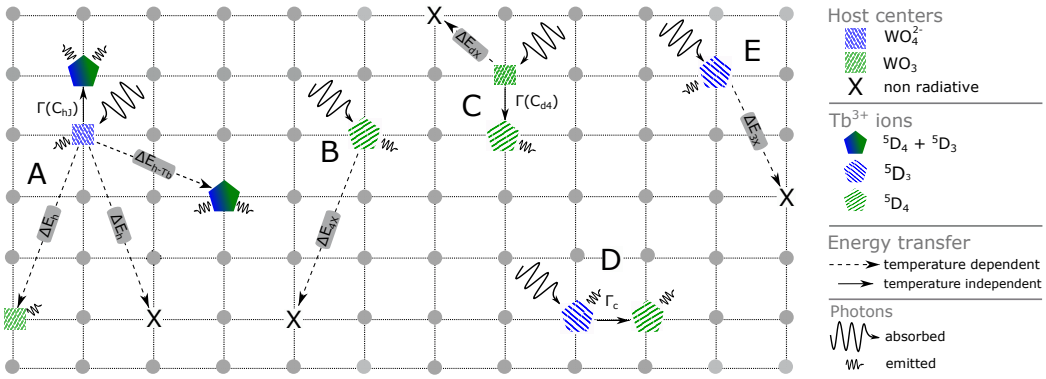

Figure 14: Sketch of $PbWO_4$:Tb^{3+} with its various energy transfer processes between the different luminescent and quenching centres. A: Excitation in WO_4^{2-} with direct energy transfer to Tb^{3+} ions and temperature induced transfer to WO_3 centres, non radiative quenching centres and Tb^{3+} ions. B: Excitation in the $^5D_4$ level of Tb^{3+}. C: Energy transfer from WO_3 to the $^5D_4$ level. D: Coupled Tb^{3+} ions showing cross relaxation. E: Isolated Tb^{3+} ions.

5 Conclusion

By measuring steady state and decay profiles as a function of temperature and concentration, a complete overview of the involved processes in the luminescence of $PbWO_4$:Tb^{3+} was obtained and depicted in Figure 14. Luminescence measurements of undoped $PbWO_4$ revealed a contribution of blue host - related emission from WO_4^{2-} centres and green defect emission from WO_3 centres. Quenching of WO_4^{2-} centres occurs via a temperature dependent energy transfer to the WO_3 defect centres and non-radiative quenching centres with a thermal energy barrier of 0.26 eV. Quenching of the green defect emission needs only a thermal energ y of 0.05 eV, however with a less steep decline. Upon doping with Tb^{3+}, new transfer paths are introduced, based on the prominent ^5D_J emission upon host excitation. At low temperature (75 K), direct energy transfer from WO_4^{2-} to neighbouring Tb^{3+} ions takes place, while transfer to less proximate Tb^{3+} ions is characterized by a thermal barrier of 0.1 eV. By contrast, the WO_3 centres show only a direct, temperature independent energy transfer to the $^5D_4$ level of Tb^{3+}.

From steady state as well as time-resolved measurements, it is clear that temperature independent cross-relaxation between the different Tb^{3+} ions induces $^5D_4$ emission upon excitation in the $^5D_3$ level. The fraction of ions taking part in this process could be calculated from the decay profiles as a function of Tb^{3+} concentration, showing a strong increase for higher dopant concentrations. Quenching of the $^5D_3$ level sets in around 350 K, corresponding with a thermal energy of 0.51 eV, compared to 400 K and 0.66 eV for the $^5D_4$ level.

The detailed analysis of the temperature dependent luminescence behavior of this particular material has shown that a multitude of phenomena are at work. A correct description and reliable extraction of energy differences from experimental data requires the identification of all relevant phenomena and is in general not straightforward, especially if multiple concentrations are considered. The use of rate equations in describing these phenomena has proven to be very useful. However, it should be noted that different processes could give rise to the same differential equations and thus no distinction between these different processes can be made with this method. In order to minimize this ambiguity, it is essential that the complete set of experimental data, i.e. thermal quenching as well as decay dynamics, and not only one aspect, is reproduced by the theoretical model, as was demonstrated here.

Parameters	$PbWO_4$	Tb concentration		
	pure	1% Tb^{3+}	2% Tb^{3+}	5% Tb^{3+}
Γ_0	$10^{14}\,s^{-1}$			
Γ_{0d}	$10^{9}\,s^{-1}$			
ΔE_h	0.26 eV			
ΔE_{dX}	0.05 eV			
Γ_{h-Tb}	–	$5.10^{10}\,s^{-1}$		
Γ_{0-Tb}	–	$10^{10}\,s^{-1}$		
Γ_4	–	$15.10^{3}\,s^{-1}$		
Γ_3	–	$3.10^{3}\,s^{-1}$		
Γ_c	–	$5.10^{4}\,s^{-1}$		
$\Gamma(C_{\mathrm{d4}})$	–	$2.10^{7}\,s^{-1}$		
ΔE_{hTb}	–	0.1 eV		
ΔE_{4X}	–	0.66 eV		
ΔE_{3X}	–	0.51 eV		
$\Gamma(C_{\mathrm{h4}})$	–	$15.10^{6}\,s^{-1}$	$30.10^{6}\,s^{-1}$	$45.10^{6}\,s^{-1}$
$\Gamma(C_{\mathrm{h3}})$	–	$20.10^{6}\,s^{-1}$	$40.10^{6}\,s^{-1}$	$60.10^{6}\,s^{-1}$
N_{iso}	–	0.95	0.85	0.35

Table 1: Obtained parameters from the fit.

Acknowledgements This research was supported by FWO (projects G039211N, G006410), Research Foundation - Flanders. J.J.J. is grateful to the agency for Innovation by Science and Technology (IWT) for financial support.

References

[1] Binnemans, K. *Coordin. Chem. Rev.* **295**, 1–45 (2015).

[2] Tanner, P. A. *Chem. Soc. Rev.* **42**(12), 5090–5101 (2013).

[3] Rabouw, F. T. and Meijerink, A. *J. Phys. Chem. C* **119**(5), 2364–2370 (2015).

[4] Bachmann, V., Ronda, C., and Meijerink, A. *Chem. Mater.* **21**(10), 2077–2084 (2009).

[5] Bunzli, J. C. G. *Coord. Chem. Rev.* **293**, 19–47 (2015).

[6] Meert, K. W., Morozov, V. A., Abakumov, A. M., Hadermann, J., Poelman, D., and Smet, P. F. *Opt. Express* **22**(9), A961–A972 (2014).

[7] Smet, P. F., Parmentier, A. B., and Poelman, D. *J. Electrochem. Soc.* **158**(6), R37–R54 (2011).

[8] Dorenbos, P. *J. Phys - Condens Mat* **15**(36), 6249 (2003).

[9] Kodaira, C., Brito, H., Malta, O., and Serra, O. *J. Lumin.* **101**(1 - 2), 11 – 21 (2003).

[10] Verhoeven, J. W. *Pure Appl. Chem.* **68**(12), 2223–2286 (1996).

[11] Barandiaran, Z., Meijerink, A., and Seijo, L. *Phys. Chem. Chem. Phys.* **17**(30), 19874–19884 (2015).

[12] Boutinaud, P. and Cavalli, E. *Chem. Phys. Lett.* **503**(4 - 6), 239 – 243 (2011).

[13] Treadaway, M. J. and Powell, R. C. *J. Chem. Phys.* **61**(10), 4003–4011 (1974).

[14] Chukova, O. and Nedilko, S. *Opt. Mater.* **35**(9), 1735–1740 (2013).

[15] Henderson, B. and Imbusch, G. *Optical Spectroscopy of Inorganic Solids.* Monographs on the physics and chemistry of materials. Clarendon Press, (1989).

[16] Bettinelli, M., Piccinelli, F., Speghini, A., Ueda, J., and Tanabe, S. *J. Lumin.* **132**(1), 27 – 29 (2012).

[17] Morozov, V. A., Bertha, A., Meert, K. W., Van Rompaey, S., Batuk, D., Martinez, G. T., Van Aert, S., Smet, P. F., Raskina, M. V., Poelman, D., Abakumov, A. M., and Hadermann, J. *Chem. Mater.* **25**(21), 4387–4395 (2013).

[18] Itoh, M. and Fujita, M. *Phys. Rev. B* **62**, 12825–12830 (2000).

[19] Groenink, J. A. and Binsma, H. *J. Solid State Chem.* **29**(2), 227–236 (1979).

[20] Groenink, J. A. and Blasse, G. *J. Solid State Chem.* **32**(1), 9–20 (1980).

[21] Takai, S., Sugiura, K., and Esaka, T. *Mater. Res. Bull.* **34**(2), 193–202 (1999).

[22] Auffray, E., Korjik, M., Shalapska, T., and Zazubovich, S. *J. Lumin.* **154**, 381–386 (2014).

[23] Mahlik, S., Cavalli, E., Bettinelli, M., and Grinberg, M. *Radiat. Meas.* **56**, 1–5 (2013).

[24] Cavalli, E., Boutinaud, P., and Grinberg, M. *J. Lumin.* **154**, 381–386 (2014).

[25] Fabeni, P., Krasnikov, A., Kärner, T., Laguta, V. V., Nikl, M., Pazzi, G. P., and Zazubovich, S. *J. Lumin.* **136**, 42–50 (2013).

[26] Kobayashi, M., Sugimoto, S., Yoshimura, Y., Usuki, Y., Ishii, M., Senguttuvan, N., Tanji, K., and Nikl, M. *Nucl. Instrum Meth A* **459**(3), 482–493 (2001).

[27] Kobayashi, M., Usuki, Y., Ishii, M., Itoh, M., and Nikl, M. *Nucl. Instrum Meth A* **540**(2-3), 381–394 (2005).

[28] Lecoq, P. *Nucl. Instrum. Meth. A* **537**(1-2), 15–21 (2005). Proceedings of the 7th International Conference on Inorganic Scintillators and their Use in Scientific adn Industrial Applications.

[29] Babin, V., Bohacek, P., Krasnikov, A., Nikl, M., Stolovits, A., and Zazubovich, S. *J. Lumin.* **124**(1), 113 – 119 (2007).

[30] Annenkov, A. A., Korzhik, M. V., and Lecoq, P. *Nucl. Instrum. Meth. A* **490**(1 - 2), 30 – 50 (2002).

[31] Nikl, M., Bohacek, P., Mihokova, E., Solovieva, N., Martini, M., Vedda, A., Fabeni, P., Pazzi, G. P., Kobayashi, M., Ishii, M., Usuki, Y., and Zimmerman, D. *J. Cryst. Growth* **229**(1), 312–315 (2001).

[32] Novosad, S. S., Kostyk, L. V., and Novosad, I. S. *J. Appl. Spectrosc.* **78**(4), 557–562 (2011).

[33] Plakhov, G. F., Pobedimskaya, E. A., Simonov, M. A., and Belov, N. V. *Sov. Phys. Crystallogr.* **15**(5), 928–929 (1971).

[34] Kubelka, P. and Munk, F. *Z. Tech. Phys. (Leipzig)* **12**, 593–601 (1931).

[35] Toyozawa, Y., Song, K., and Williams, R. *Self-Trapped Excitons*. Springer Berlin Heidelberg, (1996).

[36] Dorenbos, P. *J. Lumin.* **111**(1-2), 89–104 (2005).

[37] Joos, J. J., Poelman, D., and Smet, P. F. *Phys. Chem. Chem. Phys.* **17**, 19058 – 19078 (2015).

[38] Nikl, M., Bohacek, P., Vedda, A., Fasoli, M., Pejchal, J., Beitlerova, A., Fraternali, M., and Livan, M. *J. Appl. Phys.* **104**(9), 093514 (2008).

[39] Blasse, G. *Luminescence and Energy Transfer*, volume 42 of *Struct. Bond.*, chapter The luminescence of closed-shell transition-metal complexes. New developments, 1 – 41. Springer Berlin Heidelberg (1980).

[40] Nikl, M. *Phys. Status. Solidi. A* **178**(2), 595–620 (2000).

[41] Cavalli, E., Boutinaud, P., Mahiou, R., Bettinelli, M., and Dorenbos, P. *Inorg. Chem.* **49**(11), 4916–4921 (2010).

[42] Liao, J., Qiu, B., and Lai, H. *J. Lumin.* **129**(7), 668 – 671 (2009).

[43] Williams, R. T. and Song, K. S. *J. Phys. Chem. Solids* **51**(7), 679–716 (1990).

[44] Treadaway, M. J. and Powell, R. C. *Phys Rev B* **11**(2), 862–874 (1975).

[45] Nikl, M., Straková, P., Nitsch, K., Petricek, V., Múčka, V., Jarolímek, O., Novák, J., and Fabeni, P. *Chem. Phys. Lett.* **291**(3-4), 300–304 (1998).

[46] Förster, T. *Annalen der Physik* **437**(1-2), 55–75 (1948).

[47] Dexter, D. L. *J. Chem. Phys.* **21**(5), 836–850 (1953).

[48] Powell, R. and Blasse, G. *Energy transfer in concentrated systems*, volume 42 of *Struct. Bond.*, 43–96. Springer Berlin Heidelberg (1980).